Bulk Ultrafine-Grained Interstitial-Free Steel Processed by Equal-Channel Angular Pressing Followed by Flash Annealing

Deepa Verma, Shobhit A. Pandey, Anushka Bansal, Shwetank Upadhyay, N.K. Mukhopadhyay, G.V.S. Sastry, and R. Manna

Interstitial-free steel workpieces are deformed by equal-channel angular pressing (ECAP) for equivalent strain $\varepsilon_{vm} = 3$ and $\varepsilon_{vm} = 21$ followed by flash annealing. Microstructures are analyzed by optical microscopy, scanning electron microscopy and transmission electron microscopy. Mechanical properties are evaluated by hardness testing. Yield strength of materials is calculated from hardness values. Flash annealing (at 675 °C) of ECAPed samples for $\varepsilon_{vm} = 3$ and $\varepsilon_{vm} = 21$ results in abnormal subgrain growth and abnormal grain growth, respectively. Flash annealing at 700 °C of ECAPed (at $\varepsilon_{vm} = 3$) IF steel converts abnormally grown subgrains to grains which serve as nuclei for recrystallization and that result in bimodal grain size distribution. Bimodal grain size distribution is also produced when ECAPed IF steel for $\varepsilon_{vm} = 21$ is flash annealed at 675 °C due to abnormal grain growth or secondary recrystallization. Flash annealing of IF steel samples ECAPed for low ε_{vm}, in the temperature range 600-675 °C, decreases the hardness continuously with increase in the annealing temperature but it increases at high ε_{vm}. The former is due to annihilation of defects but the later is caused by ordering of nonequilibrium boundaries. The hardening and strengthening behaviors are similar.

1. Introduction

Interstitial-free (IF) steel is one of the recently developed steels used widely in the automotive industry because of its excellent deep drawability and high planar isotropy when the microstructure contains micrometer size grains (Ref 1) but it possesses low strength (Ref 2, 3). The strength can be improved by various strengthening methods. Most of the strengthening mechanisms lower ductility and formability. The grain size refinement is the only mechanism that improves strength with retained or improved ductility (Ref 4-6). Grain size can be reduced to ultrafine grain (UFG) range by severe plastic deformation (SPD) techniques (Ref 4, 5, 7-10). UFG steel is several times stronger than its coarse-grained counterpart, but it suffers with low ductility due to restricted dislocation activities in submicron size grained alloys (Ref 4-6). The SPD methods can produce UFGs by imposition of extremely large plastic strain to the material while preserving the initial dimensions of the workpiece (Ref 5, 7, 11, 12). Among the SPD techniques, the ECAP seems to be the most viable method because of the fact that bulk material can be deformed without any change in

cross section of the workpiece and in reasonable dimension limited by the capacity of press (Ref 8, 13-15). This technique has been applied to synthesize bulk UFG structure in IF steel sheets (Ref 2, 3, 16-21) with excellent mechanical properties (Ref 16-22). However, the UFG microstructure brought about limited ductility with a few percent uniform elongation that limits its applications (Ref 23). Previous reports have shown that the ductility of UFG materials can be enhanced without compromising the strength by appropriate annealing treatments after SPD (Ref 22-25).This improvement was attributed to the bimodal grain size distribution introduced into the deformed microstructure with the combination of fine and coarse grains (Ref 25-29). Review of UFG low carbon steel suggests that both high strength and ductility can be achieved by combining a few percentage of micron-sized (1-10 µm) grains in UFG matrix (Ref 4). In addition, the annealing synthesized can be applied also to the UFG materials processed by the SPD techniques to obtain a microstructure with enhanced stability (Ref 15). Wang et al. (Ref 26) annealed nano-grained Cu which resulted in a bimodal grain size distribution, with ~25% volume fraction of micrometer-sized grains of 1-3 µm embedded inside a matrix of ~75% volume fraction of nano-crystalline and ultrafine grains (<300 nm). Bimodal grain size distribution is reported in IF steel ECAPed for equivalent strain (ε_{vm}) 9.24 followed by annealing at 500 °C for 1 h duration due to recrystallization and coarsening of grains (Ref 2). UFG material containing ferrite and cementite microstructure with bimodal distribution of ferrite grains is reported to have a larger impact toughness compared to the material containing ferrite and pearlite, quenched and quenched and tempered martensite, in a low carbon steel (Ref 30). In case of commercial purity UFG Al, considerable efforts to introduce a bimodal grain structure failed (Ref 31), since grain coarsening occurred in a more or less homogeneous manner. The reason for this is reported as strong and rapid initial recovery and no left driving

Deepa Verma, Shobhit A. Pandey, Anushka Bansal, Shwetank Upadhyay, N.K. Mukhopadhyay, G.V.S. Sastry, and **R. Manna**, Department of Metallurgical Engineering, Indian Institute of Technology (Banaras Hindu University), Varanasi, Uttar Pradesh 221 005, India. Contact e-mails: rmanna.met@iitbhu.ac.in and rpmanna@rediffmail.com.
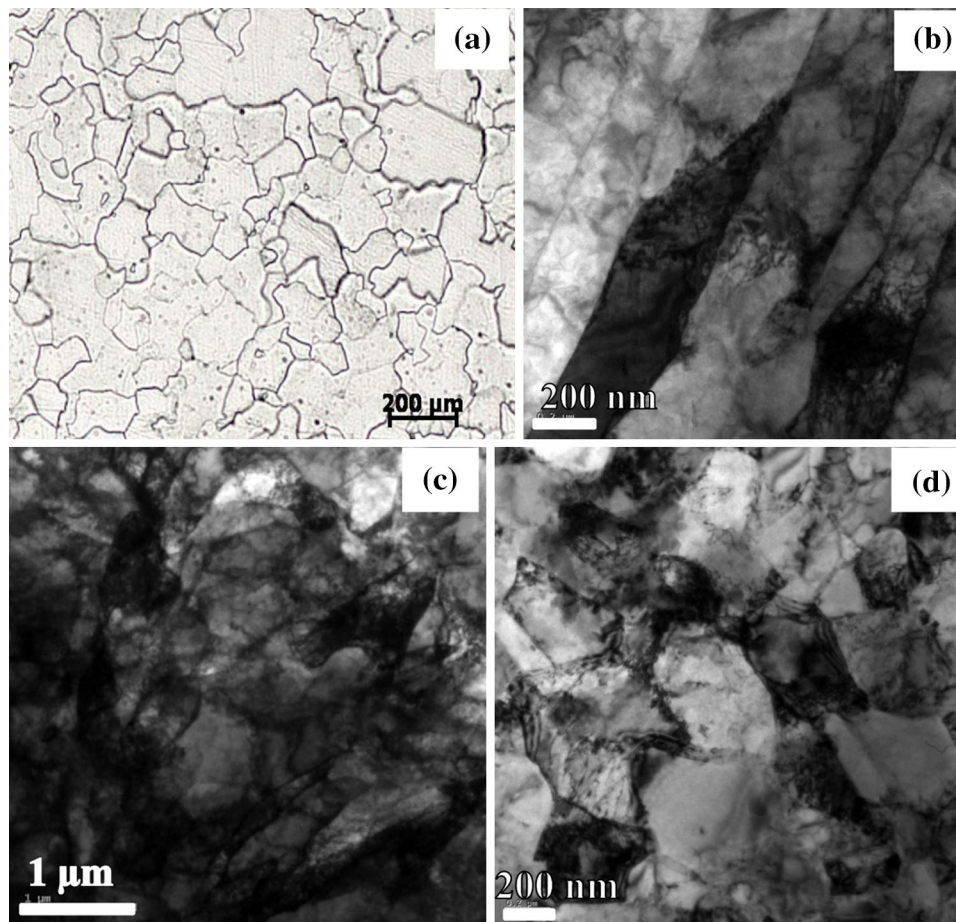
Fig. 1 (a) Optical microstructure of as-received IF steel; TEM bright field images of ECAP3 (b-c) and ECAP21 (d)

force for subsequent recrystallization, favoured by high stacking fault energy. Although some reports are available on the processing of UFG IF steel synthesized by ECAP (Ref 2, 16-19) followed by prolonged isothermal annealing treatments (Ref 16, 32), however, to the best of our knowledge, no systematic study has been published yet on the effect of flash annealing of UFG IF steel to get bimodal grain size distribution. Therefore, the present work is aimed at developing the microstructure with bimodal/multimodal grain size distribution in IF steel by ECAP followed by flash annealing.

2. Experimental Details

The workpieces of 15 mm diameter and 60 mm length are prepared from the hot-rolled plate of IF steel. The chemical composition of steel sample used for this study is C-0.0038%, Mn-0.5%, Si-0.008%, S-0.007, P-0.036, Ti-0.057, Nb-0.016%, Al-0.031% (all by wt.%) and balance is Fe. The workpieces are deformed at room temperature by the ECAP adopting the route Bc in which the sample is rotated by 90° about its axis always in one direction between two passes to obtain homogeneity in deformation (Ref 8) using a hydraulic universal testing machine of 30 ton capacity. The workpieces are coated with a lubricant mixture of high-density paraffin with MoS_2 to reduce the friction between the workpiece and the die. The ECAP die is consisted of two channels of 15 mm diameter intersecting at an

inner angle (Φ) 120° and an outer arc angle (Ψ) 60° that introduces an equivalent strain of $\sim$0.6 in every passage of the workpiece through the die. The workpieces are deformed to equivalent strains (ε_{vm}) levels of 3 and 21, and the deformed samples are designated as ECAP3 and ECAP21, respectively. The deformed samples are sectioned along Y plane for microstructural investigation. The X plane is the transverse plane perpendicular to the extrusion direction. The Y plane is the flow plane vertical to the extruded workpiece, and Z plane is the horizontal plane but parallel to the top surface along the extrusion direction (Ref 8). The ECAPed samples are flash annealed for 5 min in the 100% $NaNO_3$ melt maintained at 550-700 °C and in the air furnace at 725-750 °C followed by water quenching. The flash-annealed ECAP3 or ECAP21 samples are designated as ECAP3-FAT or ECAP21-FAT, respectively, where T indicates the temperature of annealing. The grain size of the as-received material is measured from the optical micrograph using Heyn's lineal intercept method. Thin foils of 3 mm diameter and 40 μm thickness are electropolished at -30 °C using an electrolyte of 5 vol.% perchloric acid and 95 vol.% methanol at 30 V, $\sim$60 mA. The detailed microstructures are characterized by Tecnai 20G^2 transmission electron microscope (TEM) operating at 200 kV. The annealed samples of 10×10 mm^2 are metallographically polished followed by electropolishing at 10 °C, 16 V for 40 s using 20 vol.% perchloric acid and 80 vol.% methanol. The electropolished samples are investigated in Quanta 200 FEG scanning electron microscope (SEM). The hardness is mea-
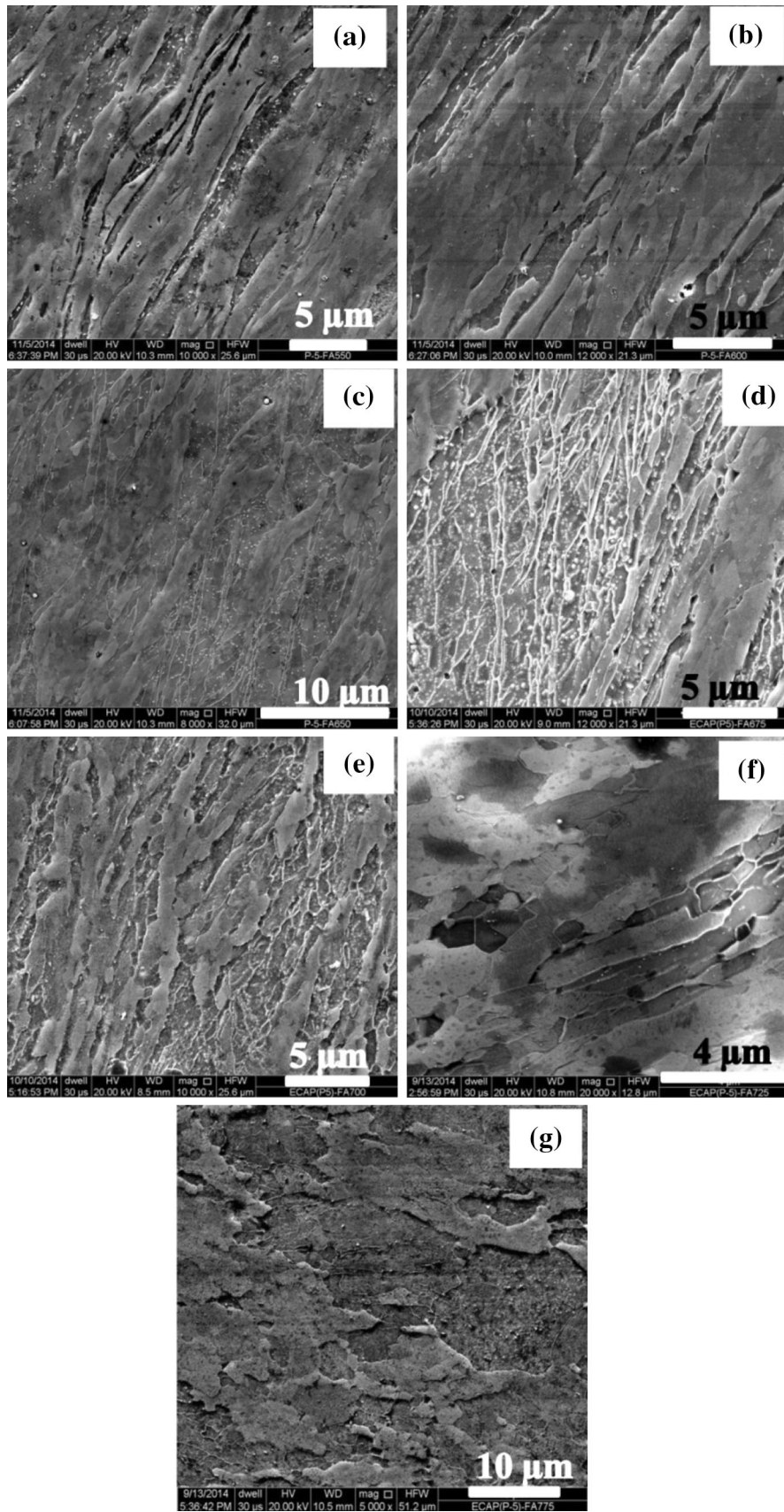
Fig. 2 SEM images of IF steel deformed up to $\varepsilon_{vm} = 3$ and flash-annealed (a) ECAP3-FA550, (b) ECAP3-FA600, (c) ECAP3-FA650, (d) ECAP3-FA675, (e) ECAP3-FA700, (f) ECAP3-FA725 and (g) ECAP3-FA750
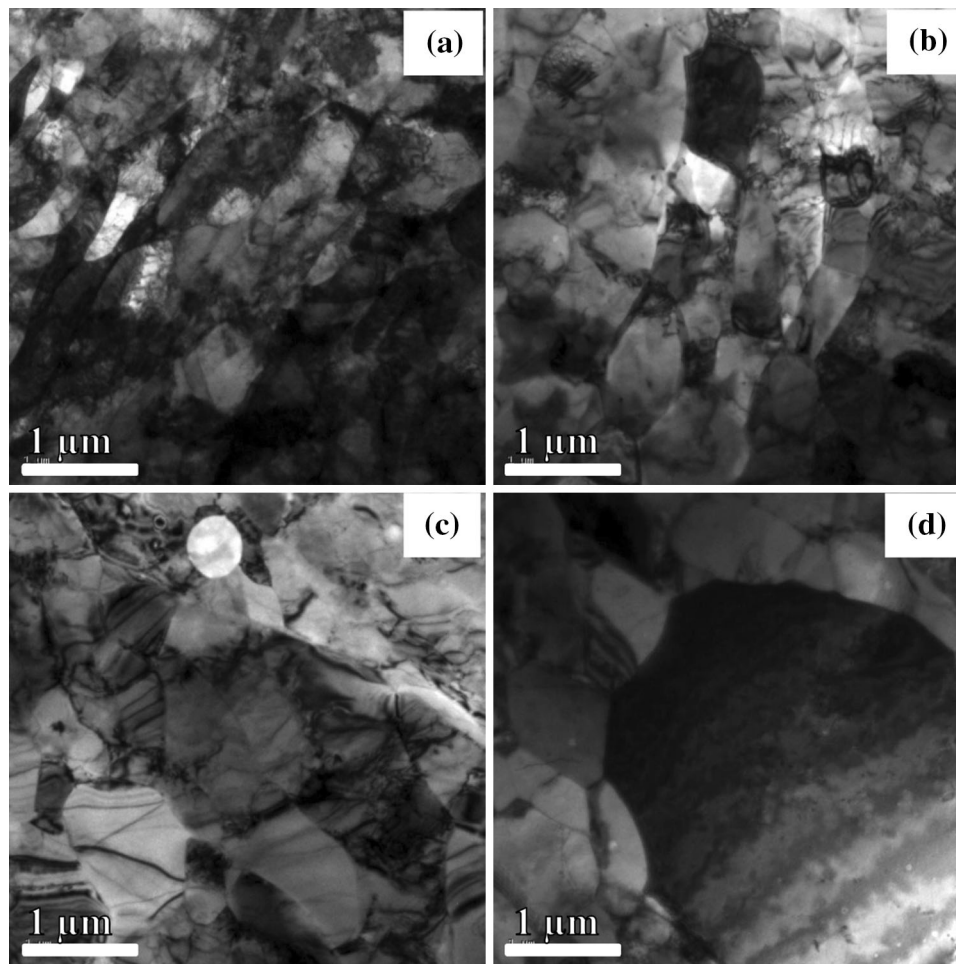
Fig. 3 TEM bright field images of IF steel deformed up to $\varepsilon_{vm} = 3$ and flash-annealed (a) ECAP3-FA675, (b) ECAP3-FA700, (c) ECAP3-FA725 and (d) ECAP3-FA750

sured by Shimadzu HMV-2T microhardness tester at 980 mN load using Vickers indenter in the extrusion plane, i.e., the Y plane of ECAPed samples. The theoritical hardness values are calculated from Hall-Petch constants (Ho and K, calculated from a fit by method of least square from experimental hardness values) within the grain size range. From the measured hardness value and tensile test data reported elsewhere (Ref 33, 34), ratio of hardness to yield strength is calculated in two regions—one in deformed state and other well-annealed state. From these ratios, yield strength is calculated for both the regions in the present experimental conditions for different flash-annealed IF steels from the theoretical harness values.

3. Results and Discussion

Figure 1(a) represents an optical micrograph of the as-received IF steel showing the microstructure of mostly equiaxed coarse-grained structure of ferrite with an average grain size of about 57.6 ± 21 μm. At $\varepsilon_{vm} = 3$, in ECAP3, coarse grains get split into deformation bands of width 298 ± 30 nm and bands get aligned toward deformation direction, which can be observed in Fig. 1(b). Some of the bands are also fragmented due to the orthogonal change in

deformation direction between two passes (Fig. 1b). Some of the dislocations get dynamically recovered during deformation and get distributed unevenly as well as tangled to form subgrain boundaries (Fig. 1c). At $\varepsilon_{vm} = 21$ (in ECAP21), Fig. 1(d) shows that the near-equiaxed ultrafine-grained structure which is developed progressively by shearing of ribbon grains and average grain size reaches 256 ± 61 nm. At low strain level, low fraction of high-angle grain boundaries exists but with increase in strain low-angle grain boundaries are being converted to the boundary of higher misorientation by progressive lattice rotation. However, a few grains still contain significant amount of dislocations. Boundaries of grains are showing some contour type structures which are indicative of their highly strained (nonequilibrium) condition (Fig. 1d).

The microstructure of ECAP3-FA550 consists of recovered banded structure of average bandwidth of 444 ± 54 nm (Fig. 2a). Annealing of ECAP3 at 600 °C, i.e., the ECAP3-FA600 sample also shows the elongated grains with the recovered banded structures of size 448 ± 35 nm (Fig. 2b). When ECAP3 sample is flash annealed at 650 °C, the morphology of grains is maintained (Fig. 2c) and the bands grow to 459 ± 87 nm by grain boundary migration. Subgrain growth is dependent on energy of low-angle grain boundaries, and growth rate is a function of subgrain misorientation (Ref 35). When the deformed samples are annealed at 675 °C, the
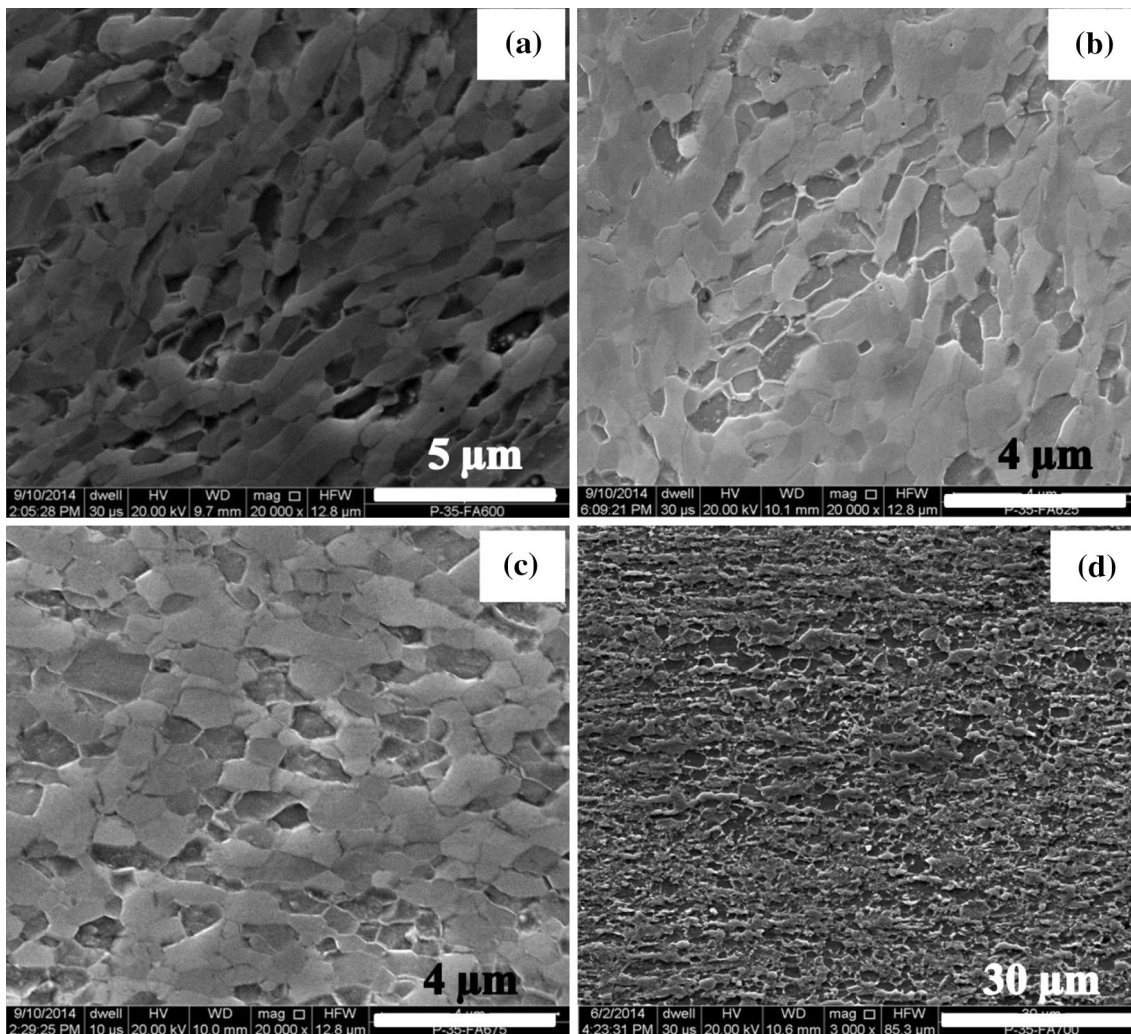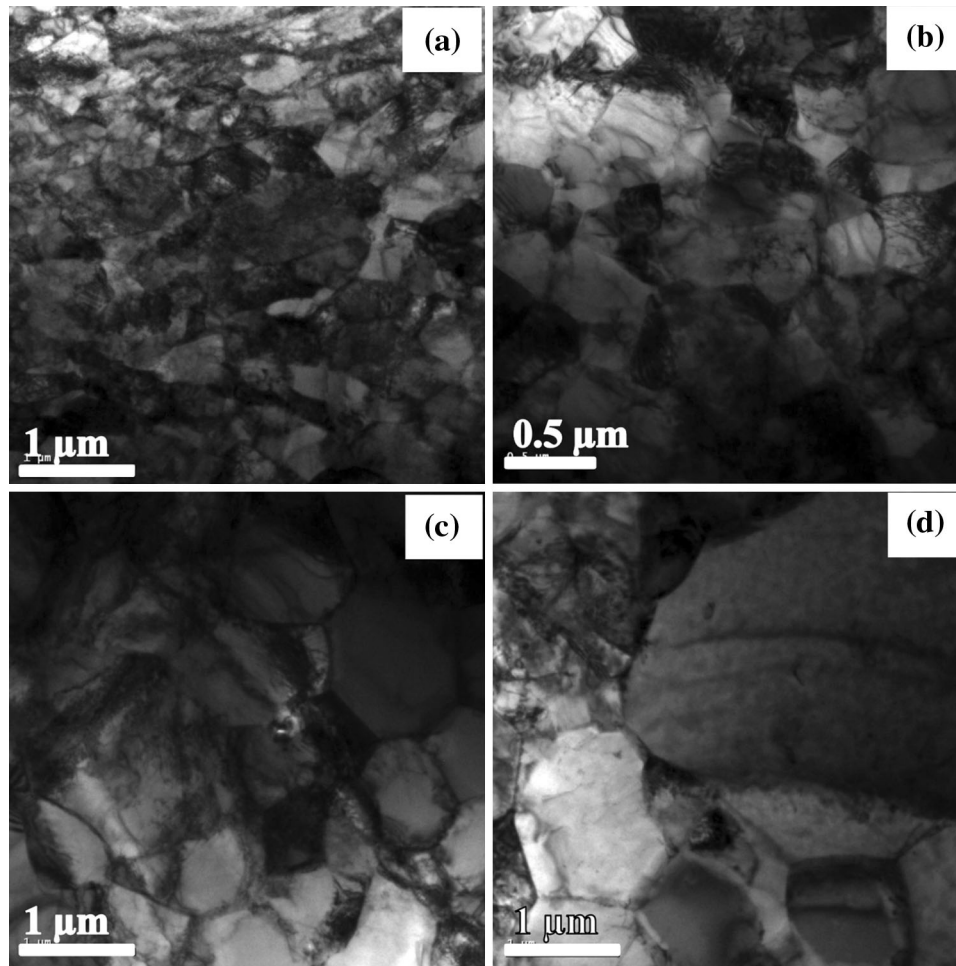
Fig. 4 SEM images of IF steel deformed up to $\varepsilon_{vm} = 21$ and flash-annealed (a) ECAP21-FA600, (b) ECAP21-FA625, (c) ECAP21-FA675 and (d) ECAP21-FA700

discontinuous subgrain growth occurs. The microstructure contains the fine subgrains of 319 ± 73 nm size along with coarse subgrains of 838 ± 20 nm (Fig. 2d, 3a). Further increasing annealing temperature to 700 °C, some of the abnormally grown subgrains eventually become grains and that leads to recrystallization. The recrystallized microstructure shows bimodal grain size distribution where equiaxed fine grains coexist with abnormally grown grains (Fig. 2e, 3b). The microstructure contains 77% fine grains of average size of 620 ± 28 nm and 23% of coarse grains of average size of 1.5 ± 0.24 μm (Fig. 2e, 3b; Table 1). On annealing of ECAP3 at 725 °C, grains are uniformly coarsened to 1.7 ± 0.38 μm (Fig. 2f, 3c). Flash annealing at 750 °C results in coarsening of grains to average size of 2.6 ± 0.36 μm (Fig. 2g, 3d).

On flash annealing of ECAP21 sample at 600 °C, fine grains increase to average size of 377 ± 94 nm (Fig. 4a, 5a) but the elongated nature is maintained. When ECAP21 sample is annealed at 625 °C, recrystallization begins and microstructure contains 93% fine grains of average size 388 ± 83 nm with 7% coarse grains of average size of 1.2 ± 0.26 μm (Fig. 4b, 5b; Table 1). On flash annealing at 675 °C, the material is recrystallized and that results in bimodal grain size distribution.

The microstructure contains 81.5% recrystallized grains of average size of 455 ± 60 nm and 18.5% of abnormally grown grains of 1.3 ± 0.21 μm (Fig. 4c, 5c). Further flash annealing at 700 °C leads to uniform coarsening of grains to 3.8 ± 0.39 μm size (Fig. 4d, 5d). Figure 6(a) represents the variation of Vickers microhardness of ECAP3 with the annealing temperature. As deformed ECAP3 sample shows the highest hardness value of 323 VHN. As this material is annealed, hardness remains at 360 VHN due to the recovery and slightly decreases to 342 VHN at 650 °C. Recovery observed after flash annealing at 550, 600, 650 °C of ECAP3 is referred to rearrangement of dislocations and formation of cell structures (as observed in Fig. 2a-c, 4a) as morphology of microstructure is not changed and most of the grains are of elongated in nature. At 675 °C, hardness value decreases to 302 VHN due to abnormal grain growth. The rate of decrease in the hardness is rapid up to 700 °C due to recrystallization and consequently the hardness value drops down to 243 VHN. The discontinuous subgrain growth is because of high-angle boundary mobility for small misorientations. Those subgrains which are slightly more misoriented than the average give rise to discontinuous subgrain growth. During plastic deformation at $\varepsilon_{vm} = 3$, high density of dislocations gets annihilated and forms subgrain and

Fig. 5 TEM images of IF steel deformed up to $\varepsilon_{vm} = 21$ and flash-annealed (a) ECAP21-FA600, (b) ECAP21-FA625, (c) ECAP21-FA675 and (d) ECAP21-FA700
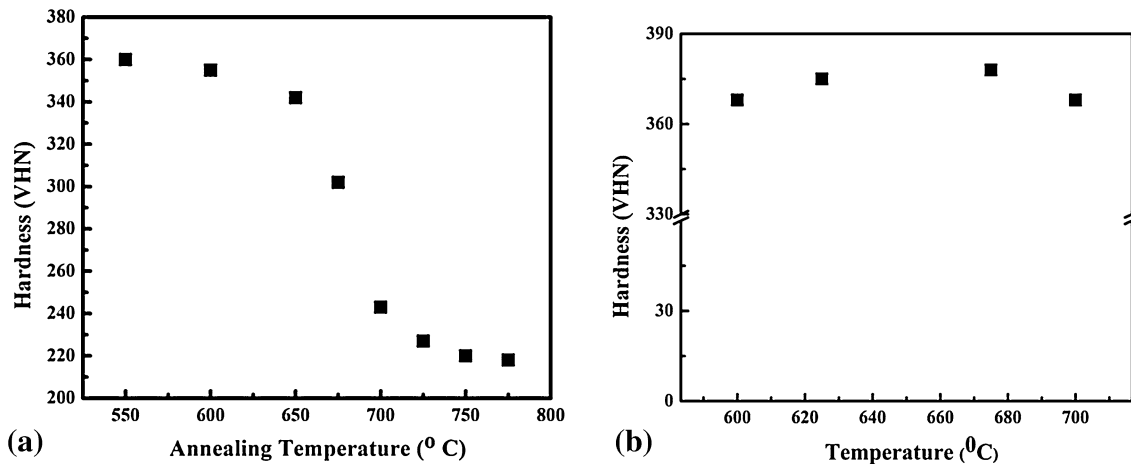

Fig. 6 Variation of hardness value with flash annealing temperature of deformed IF steel at (a) $\varepsilon_{vm} = 3$ and (b) $\varepsilon_{vm} = 21$)

cell structures. When this material is annealed, a few subgrains grow abnormally large due to nonuniform grain boundary mobility. These subgrains transform to grains and serve as nuclei for recrystallization (Ref 36). Hardness drops significantly at this stage due to rearrangement and annihilation of dislocations. The process of abnormal subgrain growth is truncated by onset of recrystallization (Ref 35) which is observed after flash annealing at 700 °C (Fig. 3b) and that results in rapid decrease in hardness (Fig. 6a). Recrystallized grains are seen to nucleate at the periphery of abnormally grown grains (Fig. 3b) where abnormally grown subgrain boundary acts as nuclei for recrystallization to occur. Nucle-
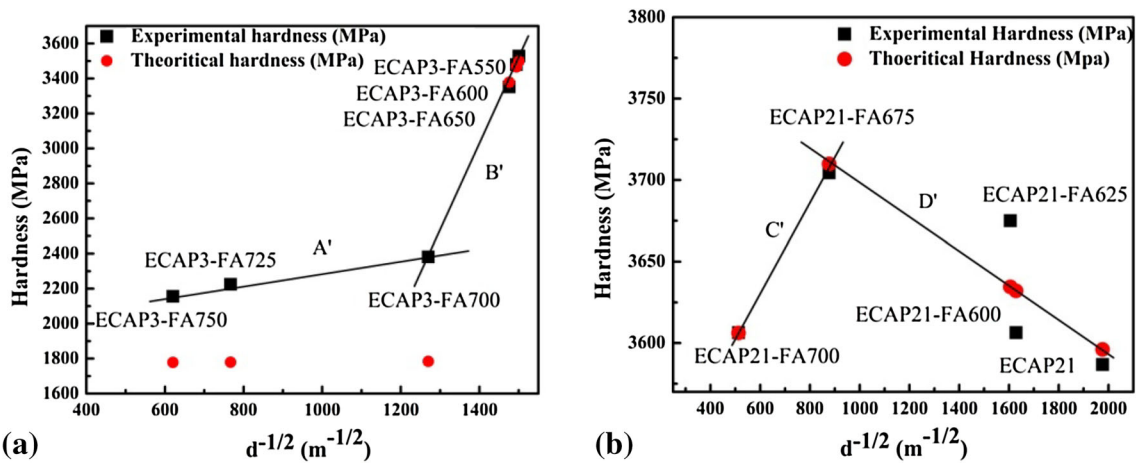
Fig. 7 Variation of hardness with inverse of grain size ($d^{-1/2}$) for flash-annealed ECAPed IF steel samples ECAPed for (a) $\varepsilon_{vm} = 3$ and (b) $\varepsilon_{vm} = 21$. Theoritical hardness values are calculated based on constants and grain size values which are indicated as red color filled circles in respective graphs
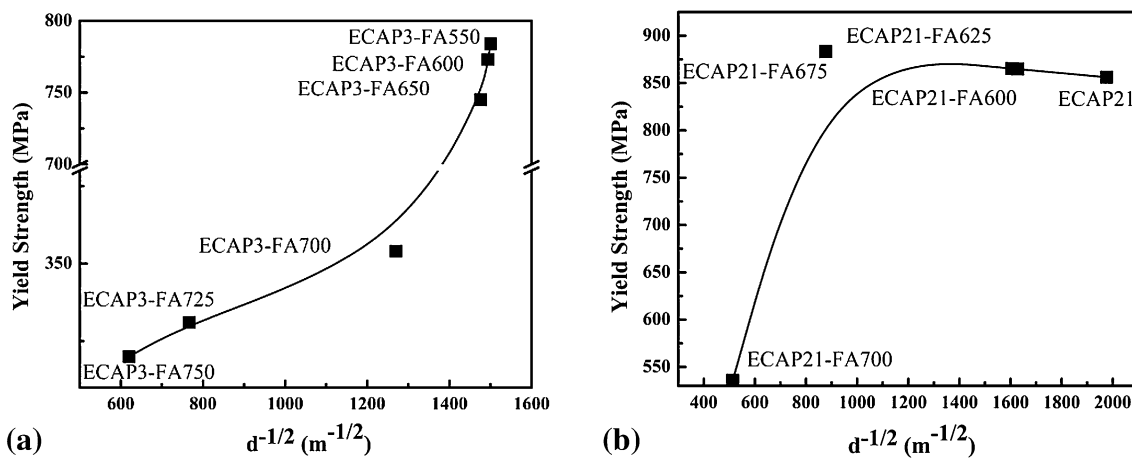
Fig. 8 Variation of calculated yield strength with grain size $^{-1/2}$ for (a) ECAP 3 category and (b) ECAP21 category IF steel samples

ation of recrystallized grains was predicted through modeling by number of workers (Ref 35, 37, 38).

Further annealing of ECAP3 at 725 °C leads to decrease in hardness to 227VHN due to coarsening of fine grains (Fig. 2f, 4d). Coarse grains grow through grain boundary migration by consuming smaller grains as coarse grains have lower relative grain boundary curvature (Ref 39, 40). Even though grain growth is observed at this temperature but effect of deformation is visible as dislocations as well as cells are present (Fig. 3c). Annealing at 750 °C brings uniform coarsening (Fig. 2f, 3d) with sharp grain boundaries. Hardness at this temperature range decreases and becomes minimum (Fig. 6a).

On flash annealing of ECAP21 at 600 °C, the recovery is observed with increased subgrain size that leaves the hardness value constant similar to that of deformed state. After the flash annealing of ECAP21 sample at 625 and 675 °C, the increase in hardness could be observed even though the grain size is more in the later case (Fig. 4b, c, 5b, c).

The relation between microhardness (H) and grain size (d) can be presented by classical Hall-Petch (H-P) equation (Ref 41, 42) as

$$H = H_0 + kd^{-1/2}$$

where H_0 is the hardness of coarse-grained material and K is gradient which is constant for material of single-phase micron-sized polycrystalline grains.

Figure 7(a) represents variation in hardness with inverse square root of grain size for IF steel samples ECAPed for $\varepsilon_{vm} = 3$ followed by flash annealing at 550-750 °C. A linear fit of method of least square from the experimental hardness values (MPa) against the inverse square root of the grain size ($d^{-1/2}$) results in a value of H_0 and K are -7160.3 MPa and 7.12 MPa m$^{1/2}$, respectively, for samples annealed at 550 to 650 °C (line B′) and 1954 MPa and 0.34 MPa m$^{1/2}$, respectively, for samples annealed at 700-750 °C (line A′). The equations which were formed by least square method are $H = 1954$ MPa $+ 0.34$ MPam1/2 $d^{-1/2}$ (for A′) and $H = -7160.3$ MPa $+7.12$ MPa m$^{1/2}$ $d^{-1/2}$ (for line B′). This indicates the mechanism of strengthening changes at 700 °C. At lower temperature, abnormal subgrain growth but above 700 °C it changes to recrystallization and normal grain growth. Whereas, fit of the experimental hardness values against the

Table 1 Details of microstructural parameters at various annealing temperatures

	Size of finer grain (nm)	% of fine grains	Coarse grain size	% of coarse grains	Grain size$^{-1/2}$ d$^{-1/2}$ (m$^{-1/2}$)	Experimental hardness (MPa)	Theoritical hardness (MPa) calculated from fit equation	Hardness to yield strength ratio	Yield Strength (MPa) (measured)
ECAP3	298±30					3171±4		4.5 (measured)	(710) (Ref 33)
Annealed UFG IF steel (recrystallized)								6.73 (measured)	(Ref 34)
ECAP3-FA550	444±54				1500.8	3528	3527	4.5	784
ECAP3-FA600	448±35				1494	3479	3479	4.5	773
ECAP3-FA650	459±87				1476	3351	3351	4.5	745
ECAP3-FA675	319±73		838±20 μm			2959			
ECAP3-FA700	620±28	77	1.5±0.24 μm	23	1270	2381	2384	6.73	354
ECAP3-FA725			1.7±0.38 μm	100	767	2227	2214	6.73	329
ECAP3-FA750			2.6±0.36 μm	100	620	2156	2164	6.73	322
ECAP21	256±61				1976.4	3587±1.6	3584	4.2 (measured)	856 (855) (Ref 33)
ECAP21-FA600	377±94	93	1.2±0.26 μm		1628.7	3606±3.6	3640	4.2	866
ECAP21-FA625	388±83				1605.4	3675±4.2	3644	4.2	865
ECAP21-FA675	455±60	81.5	1.3±0.21 μm	18.5	877	3704±3.4	3704	4.2	883
ECAP21-FA700			3.8±0.39 μm	100	513	3606±3.5	3606	6.73	536

inverse square root of the grain size gives negative slope and Hall-Petch constants H_o and K are 3801 MPa and -0.104 MPa m$^{1/2}$, respectively, in case of flash-annealed ECAP21 at 600-675 °C (line D′) (Fig. 7b). Hardness increases due to ordering of nonequilibrium boundaries which approaches toward equilibrium but it decreases when flash annealed at 700 °C due to coarsening of grains where Hall-Petch constants Ho and K become 3468 MPa and 0.26 MPa m$^{1/2}$, respectively, (line C′).

Due to limited amount of processed material, the bulk mechanical property like tensile testing could not be performed on all materials. From the measured hardness value and tensile test data reported elsewhere (Ref 33, 34), ratio of hardness to yield strength is calculated in two regions—one in deformed state and other well-annealed state. From these ratios, yield strength is calculated using measured hardness values for different flash-annealed IF steel [43]. The calculated yield strength values (Table 1) are plotted against grain size$^{-1/2}$ (Fig. 8a, b). Hardening and strengthening behaviors are similar for each type of ECAPed and flash-annealed IF steel samples.

Increase in strength after annealing is observed by many authors (Ref 44-48). Hasnaoui et al. (Ref 44) have suggested by molecular dynamic simulation that after processing, grain boundaries of nano-crystalline materials are often in a nonequilibrium state, and annealing results in grain boundaries and triple-junction regions to approach toward equilibrium which strengthens the material. Greer et al. have proposed that in small crystals, the dislocations travel smaller distance to free surface, thereby reducing the probability of dislocation multiplication processes (Ref 46). As a consequence dislocations leave the small crystals before getting multiplied and dislocation starvation region is created. After dislocation starvation conditions very high stresses are required to nucleate new dislocation and lead to increased strength (Ref 46). Hung et al. have suggested that closely spaced high-angle boundaries act as dislocation sinks to reduce the number of dislocation sources during annealing and lead to increase in the yield stress to activate new dislocation sources during straining (Ref 47). Further rising flash annealing temperature for ECAP21 to 700 °C, the grain size increases to a large value (Fig. 4d, 6b) leading to lowering of hardness.

4. Conclusions

The following conclusions can be drawn from the present investigation:

1. Equal-channel angular pressing of IF steel followed by flash annealing can be utilized to produce bimodal grain size distribution in the ultrafine grain range even though the mechanism of bimodal grain size distribution differs for different equivalent strains. Flash annealing (at 675 °C) of IF steel samples ECAPed for $\varepsilon_{vm} = 3$ and $\varepsilon_{vm} = 21$ results in abnormal subgrain growth and abnormal grain growth/secondary recrystallization. Flash annealing of lower equivalent strained sample at 700 °C converts abnormally grown subgrains to grain which serve as nuclei for recrystallization.
2. The recrystallization temperature of ultrafine-grained IF steel decreases with the increase in equivalent strain.

3. The temperature of the abnormal grain growth in IF steel increases with decrease in equivalent strain.
4. The hardness of severely deformed IF steel can be retained by flash annealing up to 650 °C for short duration of 300 s.
5. Flash annealing of IF steel samples ECAPed for high ε_{vm}, in the temperature range 600-675 °C, increases the hardness continuously with increase in the annealing temperature due to ordering of nonequilibrium boundaries toward equilibrium.
6. Hardening and strengthening behavior are similar for ECAPed IF steel.

Acknowledgments

Open Access

References

1. S.-H. Lee, H. Utsunomiya, and T. Sakai, Microstructures and Mechanical Properties of Ultra Low Carbon Interstitial Free Steel Severely Deformed by a Multi-stack Accumulative Roll Bonding Process, *Metall. Mater. Trans. A*, 2004, **45A**, p 2177–2181
2. T. Niendorf, D. Canadinc, H.J. Maier, and I. Karaman, The Role of Heat Treatment on the Cyclic Stress-Strain Response of Ultrafine-Grained Interstitial-Free Steel, *Int. J. Fatigue*, 2008, **30**, p 426–436
3. G. Purcek, O. Saray, M.I. Nagimov, A.A. Nazarov, I.M. Safarov, V.N. Danilenko, O.R. Valiakhmetov, and R.R. Mulyukov, Microstructure and Mechanical Behavior of UFG Copper Processed by ECAP Following Different Processing Regimes, *Phil. Mag.*, 2012, **92**(6), p 690–704
4. R. Song, D. Ponge, D. Raabe, J.G. Speer, and D.K. Matlock, Overview of Processing, Microstructure and Mechanical Properties of Ultrafine Grained bcc Steels, *Mater. Sci. Eng. A*, 2006, **441**, p 1–17
5. R.Z. Valiev, R.K. Islamgaliev, and I.V. Alexandrov, Bulk Nanostructured Materials from Severe Plastic Deformation, *Prog. Mater Sci.*, 2000, **45**, p 103–189
6. Y. Estrin and A. Vinogradov, Extreme Grain Refinement by Severe Plastic Deformation: A Wealth of Challenging Science, *Acta Mater.*, 2013, **61**, p 782–817
7. A.P. Zhilyaev and T.G. Langdon, Using High-Pressure Torsion for Metal Processing: Fundamentals and Applications, *Prog. Mater Sci.*, 2008, **53**, p 893–979
8. R.Z. Valiev and T.G. Langdon, Principles of Equal-Channel Angular Pressing as a Processing Tool for Grain Refinement, *Prog. Mater Sci.*, 2006, **51**, p 881–981
9. A.P. Zhilyaev, S. Lee, G.V. Nurislamova, R.Z. Valiev, and T.G. Langdon, Microhardness and Microstructural Evolution in Pure Nickel During High-Pressure Torsion, *Scr. Mater.*, 2001, **44**, p 2753–2758
10. S.H. Lee, T. Sakai, Y. Saito, H. Utsunomiya, and N. Tsuji, Strengthening of Sheath-Rolled Aluminum Based MMC by the ARB Process, *Mater. Trans. JIM*, 1999, **40**, p 1422–1428
11. R.Z. Valiev, I.V. Alexandrov, Y.T. Zhu, and T.C. Lowe, Paradox of Strength and Ductility in Metals Processed Bysevere Plastic Deformation, *J. Mater. Res.*, 2002, **17**(1), p 5–8
12. Y. Saito, H. Utsunomiya, N. Tsuji, and T. Sakai, Novel Ultra-High Straining Process for Bulk Materials—Development of the Accumulative Roll-Bonding (ARB) Process, *Acta Mater.*, 1999, **47**, p 579–583
13. X. Zhang, H. Wang, and C.C. Koch, Mechanical Behavior of Bulk Ultrafine-Grained and Nanocrystalline Zn, *Rev. Adv. Mater. Sci.*, 2004, **6**, p 53–93
14. G.J. Raab, R.Z. Valiev, T.C. Lowe, and Y.T. Zhu, Continuous Processing of Ultrafine Grained Al by ECAP-Conform, *Mater. Sci. Eng. A*, 2004, **382**, p 30–34
15. H.-S. Kim, P. Quang, M.H. Seo, S.I. Hong, K.H. Baik, H.R. Lee, and D.M. Nghiep, Process Modelling of Equal Channel Angular Pressing for Ultrafine Grained Materials, *Mater. Trans.*, 2004, **45**(7), p 2172–2176
16. S.S. Hazra, E.V. Pereloma, and A.A. Gazder, Microstructure and Mechanical Properties after Annealing of Equal-Channel Angular Pressed Interstitial-Free Steel, *Acta Mater.*, 2011, **59**, p 4015–4029
17. T. Niendorf, D. Canadinc, H.J. Maier, and I. Karaman, On the Microstructural Stability of Ultrafine-Grained Interstitial-Free Steel Under Cyclic Loading, *Metall. Mater. Trans. A*, 2007, **38A**, p 1946–1955
18. O. Saray, G. Purcek, and I. Karaman, Principles of Equal-Channel Angular Sheet Extrusion (ECASE): Application to IF-Steel Sheets, *Rev. Adv. Mater. Sci.*, 2010, **25**, p 42–51
19. H.S. Kim, W.S. Ryu, M. Janacek, S.C. Baik, and Y. Estrin, Effect of Equal Channel Angular Pressing on Microstructure and Mechanical Properties of IF Steel, *Adv. Eng. Mater.*, 2005, **7**, p 43–46
20. B. Yan, S. Dower, L. Jin, J. Shen, Y. Huang, and S. Jiao, Microstructure Evolution During Continuous Frictional Angular Extrusion of Interstitial-Free Steel, *Mater. Sci. Forum*, 2008, **584-586**, p 631–636
21. Y.H. Jin and M.Y. Huh, Evolution of Textures and Microstructures in IF-Steel Sheets During Continuous Confined Strip Shearing and Subsequent Recrystallization Annealing, *J. Mater. Sci.*, 2004, **39**, p 5311–5314
22. N. Tsuji, S. Okuno, Y. Koizumi, and Y. Minamino, Toughness of Ultrafine Grained Ferritic Steels Fabricated by ARB and Annealing Process, *Metall. Trans.*, 2004, **45**(7), p 2272–2281
23. T.S. Wang, Z. Li, B. Zhang, X.J. Zhang, J.M. Deng, and F.C. Zhang, High Tensile Ductility and High Strength in Ultrafine-Grained Low-Carbon Steel, *Mater. Sci. Eng. A*, 2010, **527**, p 2798–2801
24. Y.-H. Zhao, X.-Z. Liao, S. Cheng, E. Ma, and Y.T. Zhu, Simultaneously Increasing the Ductility and Strength of Nanostructured Alloys, *Adv. Mater.*, 2006, **18**, p 2280–2283
25. N. Tsuji, N. Kamikawa, R. Ueji, N. Takata, H. Koyama, and D. Terada, Managing Both Strength and Ductility in Ultrafine Grained Steels, *ISIJ Int.*, 2008, **48**(8), p 1114–1121
26. Yinmin Wang, Mingwei Chen, Fenghua Zhou, and En Ma, *Nature*, 2002, **419**, p 912–913
27. Y.M. Wang and E. Ma, Three Strategies to Achieve Uniform Tensile Deformation in a Nanostructured Metal, *Acta Mater.*, 2004, **52**, p 1699–1709
28. A.H. Shamdani, S. Khoddam, P.F. Thomson, and A. Dehghan-Manshadi, Microstructure and Mechanical Properties of IF Steel Deformed During Plane Stress Local Torsion, *J. Mater. Sci.*, 2012, **47**(3), p 1582–1587
29. Y.-H. Zhao, T. Topping, J.F. Bingert, J.J. Thornton, A.M. Dangelewicz, Y. Li, W. Liu, Y. Zhu, Y. Zhou, and E.J. Lavernia, High Tensile Ductility and Strength in Bulk Nanostructured Nickel, *Adv. Mater.*, 2008, **20**, p 3028–3033
30. T. Hanamura, F. Yin, and K. Nagai, Ductile-Brittle Transition Temperature of Ultrafine Ferrite/Cementite Microstructure in a Low Carbon Steel Controlled by Effective Grain Size, *ISIJ Int.*, 2004, **44**(3), p 610–617
31. H. Mughrabi, H.W. Hoppel, and M. Kautz, Fatigue and Microstructure of Ultrafine-Grained Metals Produced by Severe Plastic Deformation, *Scr. Mater.*, 2004, **51**, p 807–812
32. G. Purcek, O. Saray, I. Karaman, and H.J. Maier, High Strength and High Ductility of Ultrafine-Grained, Interstitial-Free Steel Produced by ECAE and Annealing, *Metal. Mater. Trans. A*, 2012, **43**(6), p 1884–1894
33. D. Verma, N.K. Mukhopadhyay, G.V.S. Sastry, and R. Manna, Ultra-High-Strength Interstitial-Free Steel Processed by Equal-Channel

Angular Pressing At Large Equivalent Strain, *Metall. Mater. Trans. A*, 2016, **47**, p 1803–1817

34. D. Verma, N.K. Mukhopadhyay, G.V.S. Sastry, R. Manna, Microstructure and Mechanical Properties of Ultrafine-Grained Interstitial-Free Steel Processed by ECAP. Trans. Indian. Inst. Met. (2016). doi: 10.1007/s12666-016-0881-0

35. F.J. Humphreys and M. Hatherly, *Recrystallization and Related Annealing Phenomena*, 2nd ed., Pergamon Press, Oxford, 1995, p 192–200

36. E.A. Holm, M.A. Miodownik, and A.D. Rollett, On Abnormal Subgrain Growth and the Origin of Recrystallization Nuclei, *Acta Mater.*, 2003, **51**, p 2701–2716

37. A.D. Rollett, E.A. Holm, T.R. McNelley (ed.), Recrystallization 96, TMS, Warrendale, PA, 1996, p 31–42

38. F.J. Humphreys, A Unified Theory of Recovery, Recrystallization and Grain Growth, Based on the Stability and Growth of Cellular Microstructures—I. The Basic Model, *Acta Mater.*, 1997, **45**, p 4231–4240

39. R.G. Cawthorn, *Layered Intrusions*, Elsevier, Amsterdam, 1996, p 91

40. C. Antonione, G. Della Gatta, G. Riontino, and G. Venturello, Grain Growth and Secondary Recrystallization in Iron, *J. Mater. Sci.*, 1973, **8**, p 1–10

41. E.O. Hall, The Deformation and Aging of Mild Steel: III. Discussion of Results, *Proc. Phys. Soc. B*, 1951, **64**, p 747–753

42. N.J. Petch, The Cleavage Strength of Polycrystals, *J. Iron Steel Inst.*, 1953, **174**, p 25–28

43. P. Zhang, S.X. Li, and Z.F. Zhang, General Relationship Between Strength and Hardness, *Mater. Sci. Eng. A*, 2011, **529**, p 62–73

44. A. Hasnaoui, H. Van Swygenhoven, and P.M. Derlet, On Non-equilibrium Grain Boundaries and Their Effect on Thermal and Mechanical Behaviour: A Molecular Dynamics Computer Simulation, *Acta Mater.*, 2002, **50**, p 3927–3939

45. A. Torrents, H. Yang, and F. Mohamed, Effect of Annealing on Hardness and the Modulus of Elasticity in Bulk Nanocrystalline Nickel, *Metall. Mater. Trans. A*, 2010, **41**(3), p 621–630

46. J.R. Greer, W.C. Oliver, and W.D. Nix, Size Dependence of Mechanical Properties of Gold at the Micron Scale in the Absence of Strain Gradients, *Acta Mater.*, 2005, **53**, p 1821–1830

47. X. Huang, N. Hansen, and N. Tsuji, Hardening by Annealing and Softening by Deformation in Nanostructured Metals, *Science*, 2006, **312**, p 249–251

48. N. Kamikawa, X. Huang, N. Tsuji, and N. Hansen, Strengthening Mechanisms in Nanostructured High-Purity Aluminium Deformed to High Strain and Annealed, *Acta Mater.*, 2009, **57**, p 4198–4208